Regenerative Therapy 25 (2024) 220–228

Contents lists available at ScienceDirect

Regenerative Therapy

journal homepage: http://www.elsevier.com/locate/reth

Original Article

Evaluation of adipogenesis over time using a novel bioabsorbable implant without the addition of exogenous cells or growth factors

Sunghee Lee [a], Shuichi Ogino [b, *], Yoshihiro Sowa [a], Kenta Yamamoto [c], Yuki Kato [d], Maria Chiara Munisso [a], Susumu Saito [a], Manabu Shirai [e], Tetsuji Yamaoka [f], Naoki Morimoto [a]

[a] Department of Plastic and Reconstructive Surgery, Graduate School of Medicine, Kyoto University, Kyoto, Japan
[b] Department of Plastic and Reconstructive Surgery, Shiga University of Medical Science, Shiga, Japan
[c] Department of Immunology, Kyoto Prefecture University of Medicine, Kyoto, Japan
[d] Gunze QOL Research Center Laboratory, Kyoto, Japan
[e] Omics Research Center (ORC), National Cerebral and Cardiovascular Center, Osaka, Japan
[f] Department of Biomedical Engineering, National Cerebral and Cardiovascular Center Research Institute, Osaka, Japan

ARTICLE INFO

Article history:
Received 11 October 2023
Received in revised form
25 November 2023
Accepted 21 December 2023

Keywords:
Adipogenesis
Bioabsorbable
Breast cancer
Multiphoton excitation fluorescence microscopy

ABSTRACT

Background: Breast reconstruction is crucial for patients who have undergone mastectomy for breast cancer. Our bioabsorbable implants comprising an outer poly-L-lactic acid mesh and an inner component filled with collagen sponge promote and retain adipogenesis *in vivo* without the addition of exogenous cells or growth factors. In this study, we evaluated adipogenesis over time histologically and at the gene expression level using this implant in a rodent model.
Methods: The implants were inserted in the inguinal and dorsal regions of the animals. At 1, 3, 6, and 12 months post-operation, the weight, volume, and histological assessment of all newly formed tissue were performed. We analyzed the formation of new adipose tissue using multiphoton microscopy and RNA sequencing.
Results: Both in the inguinal and dorsal regions, adipose tissue began to form 1 month post-operation in the peripheral area. Angiogenesis into implants was observed until 3 months. At 6 months, microvessels matured and the amount of newly generated adipose tissue peaked and was uniformly distributed inside implants. The amount of newly generated adipose tissue decreased from 6 to 12 months but at 12 months, adipose tissue was equivalent to the native tissue histologically and in terms of gene expression.
Conclusions: Our bioabsorbable implants could induce normal adipogenesis into the implants after subcutaneous implantation. Our implants can serve as a novel and safe material for breast reconstruction without requiring exogenous cells or growth factors.

1. Introduction

In recent years, the number of patients with breast cancer has increased. Standard treatments include autologous composite tissue reconstruction, silicone implants, and autologous fat grafting. However, these methods pose several issues, including surgical invasion, scar, necrosis, infection, capsular contracture [1,2], implant rapture [1,2], breast implant-associated anaplastic large cell lymphoma [3,4], and the low survival rate of grafted fat [5,6]. Therefore, there is an urgent need to develop and implement new treatments to solve these issues and preserve the quality of life of patients with breast cancer.

Tissue engineering aims at regenerating tissues and organs in combination with scaffolds [7,8], growth factors [9,10], and cells

Abbreviations: ASCs, adipose tissue-derived stem cells; CS, collagen sponge; PLLA, poly-l-lactic acid; RNA-seq, RNA sequencing; OCT, optimum cutting temperature; H and E, hematoxylin and eosin.

* Corresponding author. Department of Plastic and Reconstructive Surgery, Shiga University of Medical Science, Seta Tsukinowa-cho, Otsu, Shiga 520-2192, Japan.
E-mail addresses: nami0128@kuhp.kyoto-u.ac.jp (S. Lee), sogino12@belle.shiga-med.ac.jp (S. Ogino), sowawan@kuhp.kyoto-u.ac.jp (Y. Sowa), fiori30@koto.kpu-m.ac.jp (K. Yamamoto), yuuki.kato@gunze.co.jp (Y. Kato), munisso@kuhp.kyoto-u.ac.jp (M.C. Munisso), susumus@kuhp.kyoto-u.ac.jp (S. Saito), shirai.manabu.ri@ncvc.go.jp (M. Shirai), yamtet@ncvc.go.jp (T. Yamaoka), mnaoki22@kuhp.kyoto-u.ac.jp (N. Morimoto).

Peer review under responsibility of the Japanese Society for Regenerative Medicine.

https://doi.org/10.1016/j.reth.2023.12.015

[11,12]. Adipose tissue-derived stem cells (ASCs), with self-renewal and pluripotent differentiation potential, are a major source of cells for tissue engineering and regenerative medicine. Adipose tissue is a major source of ASCs and mature adipocytes [13–17]. In clinical application, the addition of ASCs to fat grafts improves the survival rate [18,19]. However, there is no clear consensus on the effects of ASCs on tumor growth or the safety of these therapies in patients with cancer [20].

Regarding the clinical formation of adipose tissue, fat degeneration of the muscle and bone marrow, as well as ectopic fat accumulation, are commonly encountered. In plastic and reconstructive surgery, infantile hemangiomas grow throughout the first year of life and then disappear, sometimes replaced by adipose tissue during degeneration or regression [21,22]. However, the mechanism underlying fat degeneration has not yet been clarified. We hypothesized that the maintenance of internal space is the main factor for adipose tissue regeneration *in vivo*.

In our previous study [23], we found that adipose tissue was formed in a cage made of polypropylene mesh filled with collagen sponge (CS) without growth factors or ASCs. Next, we developed novel implants that combined a poly-L-lactic acid (PLLA) mesh with CS, which were bioabsorbable in a few years and did not require removal. We have already shown that this implant can generate autologous adipose tissue without the addition of cells or growth factors one year after implantation [24]. However, the adipogenesis over time after implantation has not yet been elucidated.

In this study, we inserted our implants subcutaneously into the inguinal region, where there was a lot of native adipose tissue, and the dorsal region, where there was little or no adipose tissue, and compared the adipogenesis into implants over time within one year. In addition, we evaluated the newly formed adipose tissue morphologically using multiphoton microscopy and evaluated adipogenesis- and angiogenesis-related gene expression using RNA sequencing (RNA-seq).

2. Material and methods

2.1. Preparation of the bioabsorbable implants

In this study, we prepared 80 implants made of PLLA containing CS (CS; PELNAC®, Gunze Ltd., Tokyo, Japan), as previously reported [24]. First, a 2-0 PLLA thread was woven into a columnar mesh. Next, after stuffing with 40 mm × 20 mm × 3 mm CS with a porosity of 80–95 %, the top and bottom of the mesh were closed by suturing with purse strings. The maximum diameter of the short axis, the equatorial diameter of the sphere, was approximately 7.5 mm, and the maximum length of the long axis, which is the distance between the poles of the symmetry axis, was approximately 18 mm. On the implant surface, the gaps between the mesh were squares measuring approximately 1.5 × 1.5 mm (Fig. 1a).

2.2. Animal experiments

2.2.1. Experimental design and operative procedures

Male F344/Jcl rats (10 weeks old, n = 20) were purchased from CLEA Japan Inc. (Osaka, Japan). These animals were used because they are inbred, thus eliminating individual differences, and their physiological cycles are unaffected. The sample size was determined following our previous studies using the rat model [24]. The implants were inserted subcutaneously on both sides of the inguinal (n = 40) and dorsal (n = 40) regions. For the inguinal model, the following procedure was performed: after shaving and depilating the inguinal region, a 2 cm long skin incision was made at the cranial part of the inguinal ligament. The inguinal fat pad was incised and a pocket was prepared to accommodate the implant underneath the fat pad. The implant was subsequently placed in the pocket above the femoral vessels and fixed to the fat pad using 4-0 nylon sutures (Diadem: Wonderworks Inc., Tokyo, Japan). Finally, the fat pad and skin were closed with 4-0 nylon sutures. The left and right sides were treated similarly, and thus a total of two implants were inserted for each animal. In the dorsal model, we performed the following steps: a skin incision of 3 cm was made in the middle of the back, located 2 cm caudal to the axilla and 5 cm cranial to the iliac crest. After the pocket was made under fascia, the implant was inserted into the pocket and fixed to the muscle with 4-0 nylon sutures. The facia and skin were closed with 4-0 nylon sutures. The left and right sides were treated similarly, with two implants inserted in each animal.

2.2.2. Evaluation of weight and volume of all newly formed tissues

For histological tissue evaluation, three rats were euthanized by carbon dioxide inhalation at 1, 3, 6, and 12 months after the operation, and both the inguinal and dorsal samples were evaluated (n = 6). Rats to be sacrificed were decided randomly, and not arbitrarily. In the inguinal model, all newly formed tissues, including implants, were harvested from the iliac crest to the midline above the muscle layer in the abdominal region and the section above the muscle layer in the femoral region. In the dorsal model, all newly formed tissues, including the implant, were harvested above the fascia located 2 cm caudal to the axilla, 5 cm cephalad to the iliac crest, and bounded by the lateral midline and the midline. The harvested specimens were weighed on an electronic balance (PM4600, Mettler-Toledo International Inc., Tokyo, Japan), and the sample volume was measured using a standard water displacement technique [25].

2.2.3. Histological assessment of the newly generated tissue inside the implants

Harvested specimens were fixed in a 10 % formalin neutral buffer solution (FUJIFILM Wako Pure Chemical Industries, Corporation, Osaka, Japan). In the inguinal model, the implant from each specimen was divided into four equal parts along the long axis (Fig. 1b). The second block from the medial side was embedded in the optimum cutting temperature (OCT) compound (Sakura Fine Technical Co. Ltd, Tokyo, Japan) and frozen in ethanol at −30 °C for multiphoton imaging. The other three blocks were paraffin-embedded. In the dorsal model, the implant from each specimen was divided into four equal parts along the long axis (Fig. 1c). The second block from the upper side was embedded in an OCT compound and frozen in ethanol at −30 °C for multiphoton imaging. The remaining three blocks were embedded in paraffin. The 3 μm paraffin sections were prepared for hematoxylin and eosin (H and E) and immunohistochemical staining. All images were captured at 40x magnification using Keyence BZ-X810 (KEYENCE Co., Tokyo, Japan). Experimental data were analyzed by blinded researchers who did not know the details of the implants. With the hypothesis if the number of samples is 10, there is a significant difference, n = 10 (n = 6 for histological evaluation, n = 4 for RNAseq) both for the inguinal and dorsal region for each period.

2.2.4. Immunohistochemistry

Immunohistochemical staining of perilipin (Perilipin-1 [D1D8] XP® Rabbit mAb #9349; Cell Signaling Technology, Danvers, Massachusetts) was performed to evaluate the newly generated tissues and adipose tissues inside the implant. The sections were imaged using a Keyence BZ-X810 at 40x magnification. The area of the newly generated tissue within each implant and the newly generated adipose tissue within each implant were evaluated using Fiji [26] (Fig. 2). The average area of the three sections was used for the statistical evaluation.

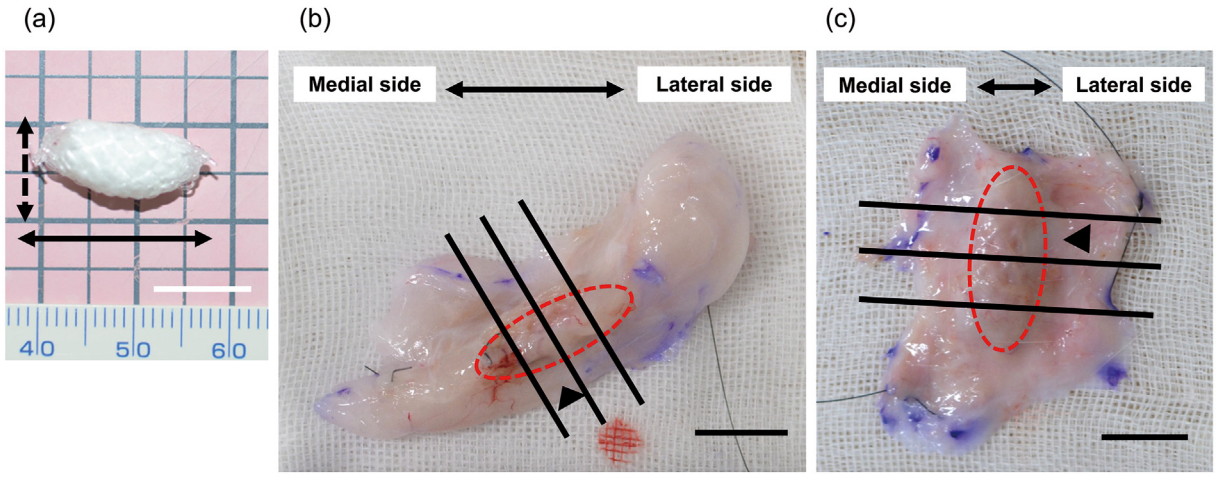

Fig. 1. (a) Gross appearance of the implant. The implant consisted of a PLLA mesh with a CS. The dashed black arrow indicates the greatest diameter of the short axis of the implant, and the solid black arrow indicates the greatest length of the long axis of the implant. (b) Histological assessment of newly generated tissue in the inguinal model. (c) Histological assessment of newly generated tissue in the dorsal model. The area circled by the red dotted line represents the implant shape. The implant was divided into four equal parts along the long axis, as shown by the straight black line. The black arrowhead indicates the frozen specimen. Scale bar = 1 cm.

Immunohistochemical staining with anti-CD31 antibody (Anti-CD31 [EPR17259] Rabbit Monoclonal Antibody ab182981; Abcam plc, Cambridge, UK) was performed to evaluate angiogenesis inside the implants. The sections were imaged using the Keyence BZ-X810 at 40x magnification.

2.2.5. Multiphoton imagining of the newly generated adipose tissue

The surface of the central cross-section of the implant was evaluated 6 and 12 months after the operation. The inguinal subcutaneous adipose tissue and a sample of the native adipose tissue of a 6-month-old male F344/Jcl rat were harvested. Frozen specimens were thawed at room temperature to remove OCT compounds and washed with PBS. They were then stained with the three dyes. The nuclei were stained with Hoechst33342 (cat. No. H3570, Invitrogen, Waltham, Massachusetts); the blood vessels with isolectin GS-IB_4 from *Griffonia simplicifolia*, Alexa Fluor™ 488 conjugate (cat. No. 121411, Invitrogen, Waltham, MA, USA); and the adipose tissue was treated with Nile Red (cat. No. N1142, FUJIFILM Wako Pure Chemical Corporation, Osaka, Japan). Finally, after washing with PBS, the stained specimens were observed using an Olympus FVMPE-RS multiphoton microscope equipped with a Spectra-Physics Ti:Sapphire laser (Mai Tai® DeepSee; Spectra-Physics, Santa Clara, CA, USA). Multiphoton images were acquired using 10x (UPLXAP010X, NA 0.4×; Olympus, Tokyo, Japan) and 30× silicon oil-immersion objectives (UPLSAPO30XSIR, NA 1.05; Olympus, Tokyo, Japan). The laser power was kept constant at 2 mW, and two excitation wavelengths, 860 nm and 760 nm, were used. At 860 nm, SHG images arising from the collagen fibers were detected through a 420–460-nm filter (FV30-FVG; Olympus), the blood vessel images through a 495–540-nm filter (FV30-FGR; Olympus), and the adipose tissue images through a 575–630-nm filter (FV30-FCY; Olympus). The same areas were imaged at 760 nm, with the nuclear images collected at 420–460 nm, the blood vessels at 495–540 nm, and the adipose tissue at 575–630 nm.

2.2.6. RNA-seq

For RNA-seq evaluation, the dorsal samples of two rats (n = 4) were evaluated at 1, 3, 6, and 12 months after the implant operation. Total RNA was extracted using the RNeasy Plus Universal Mini Kit (QIAGEN Inc., Valencia, CA, USA). RNA integrity number was measured using the Agilent 4200 TapeStation (Agilent, Santa Clara, USA) to assess the quality of isolated total RNA from each implant.

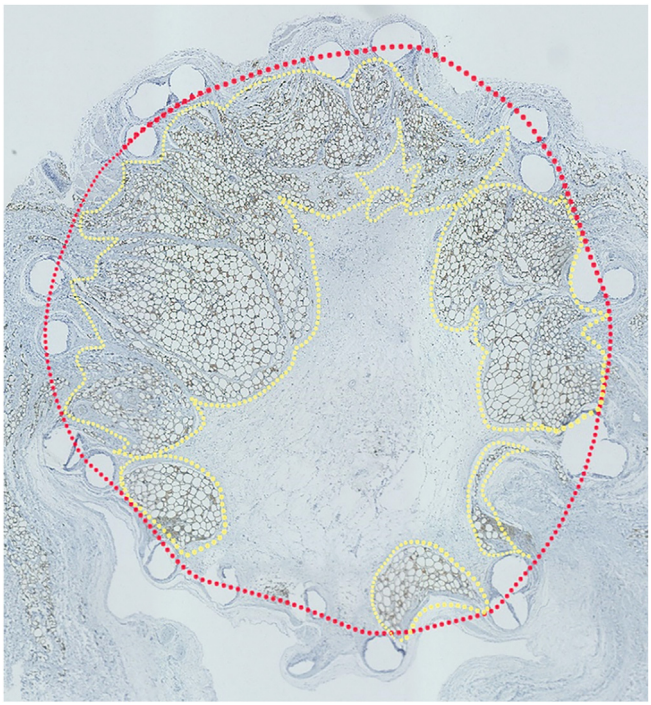

Fig. 2. Evaluation of the area of newly generated tissue and adipose tissue inside the implants. The red dotted line shows the implant area, and the yellow dotted line shows the area of new adipose tissue inside the implants.

mRNA sequencing (mRNA-seq) libraries from high-quality total RNA were prepared using the TruSeq stranded mRNA library prep kit (Illumina, San Diego, USA). After evaluation of library quality, sequencing was performed with 75 bp singe-end reads using NextSeq 500 High Output kit (Illumina). The acquired sequence data was aligned to rat rn6 built, annotated rat RefSeq transcripts, and analyzed using Strand NGS software (Agilent Technologies).

2.3. Statistical analysis

Differences between samples were examined for statistical significance by analysis of variance and the Tukey–Kramer test. All

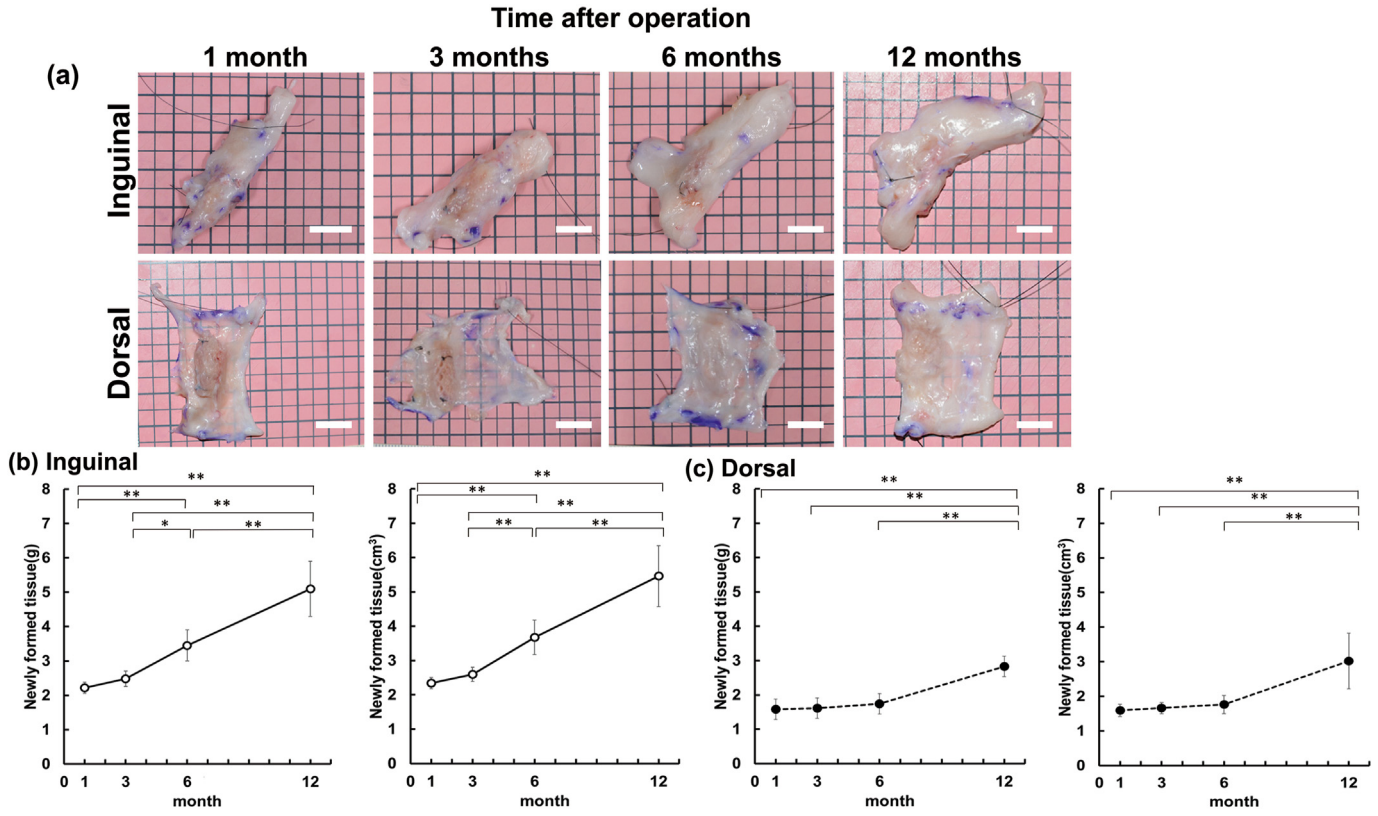

Fig. 3. Weight and volume of all the newly formed tissues. (a) Gross appearance of all newly formed tissues. At the time of the operation, there was little adipose tissue in the dorsal region. As the rats grew, the subcutaneous area became entirely covered with adipose tissue. Upper row: inguinal model; lower row: dorsal model. Scale bar = 1 cm. (b) Time course of the weight and volume of all newly formed tissues in the inguinal model. In both the inguinal model and the dorsal model, the weight at 12 months was the heaviest and largest. Left graph: shows the time course of weight trend; right graph: the time course of the volume trend. Data are presented as the mean ± standard deviation. $*p < 0.05$, $**p < 0.01$. (c) Time course of the weight and volume of all newly formed tissues in the dorsal model. In both the inguinal model and the dorsal model, the volume at 12 months was the heaviest and largest. Left graph: the time course of weight; right graph: the time course of the volume. Data are presented as the mean ± standard deviation. $*p < 0.05$, $**p < 0.01$.

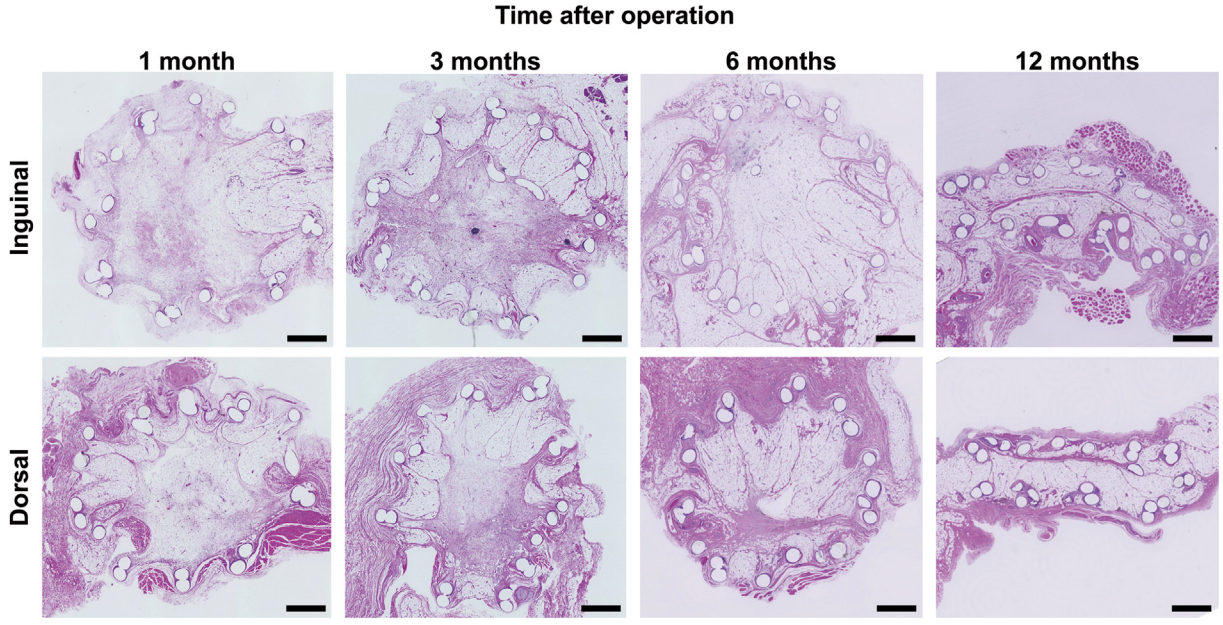

Fig. 4. Light micrographs of H and E-stained sections of the newly regenerated tissue. In both the inguinal and dorsal models, the implant shape could be maintained for up to 6 months after the operation. Upper row: light micrographs in the inguinal model; lower row: light micrographs in the dorsal model. Scale bar = 1 cm.

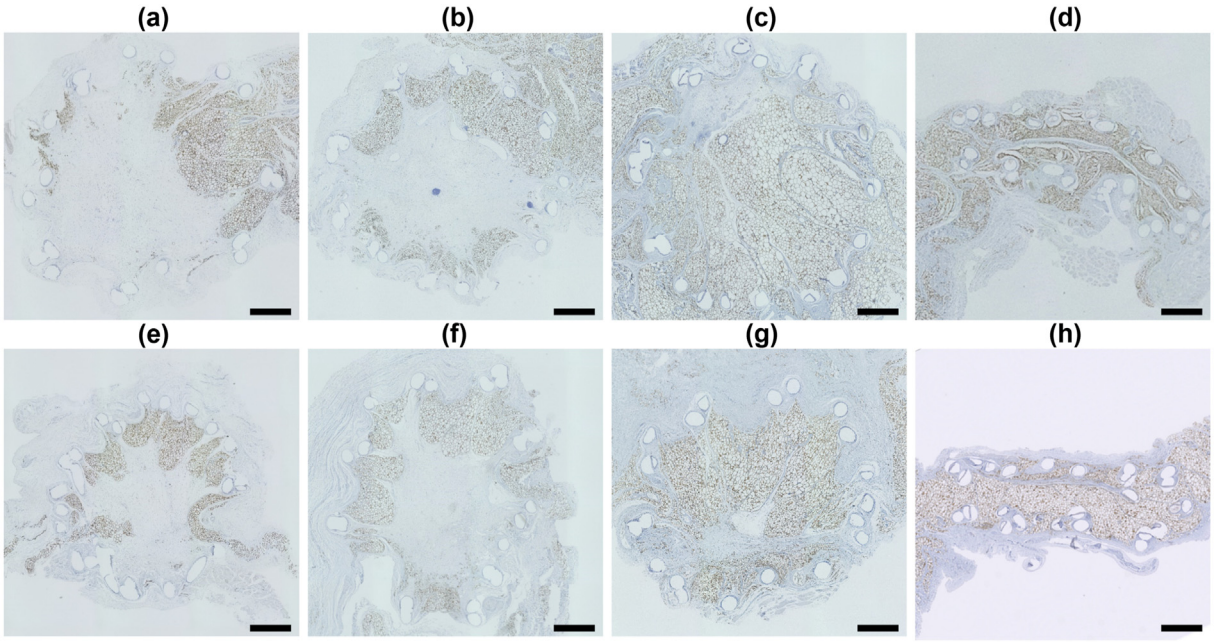

Fig. 5. Light micrographs of perilipin-stained sections of the newly generated tissue. In both the inguinal and dorsal models, the adipose tissue gradually increased from the edge of the implant after the operation. Upper row: light micrographs in the inguinal model. (a) 1 month, (b) 3 months, (c) 6 months, (d) 12 months after the operation. Lower row: light micrographs in the dorsal model. (e) 1 month, (f) 3 months, (g) 6 months, (h) 12 months after the operation. Scale bar = 1 cm.

data are expressed as the mean ± standard deviation, and *p*-values <0.05 were considered statistically significant. Microsoft Excel along with Statcel3 add-in (Oms Publishing Inc., Tokyo, Japan) was used for all statistical analyses.

3. Results

3.1. Evaluation of weight and volume of all newly formed tissues

During the postsurgical follow-up period, infection, hematoma, and tumor formation were not observed. Representative images of newly formed tissues at 1, 3, 6, and 12 months after the operation are shown in Fig. 3a. All newly formed tissues became larger over time. At the time of the operation, there was little adipose tissue in the dorsal region; however, as the rats grew, the subcutaneous area became entirely covered with adipose tissue. The PLLA threads were microscopically visible in all samples up to 12 months after the operation. The time courses of weight and volume for all newly formed tissues in the inguinal and dorsal models are shown in Fig. 3b and c, respectively. In both the inguinal model and the dorsal model, the weight and volume at 12 months were heaviest and largest.

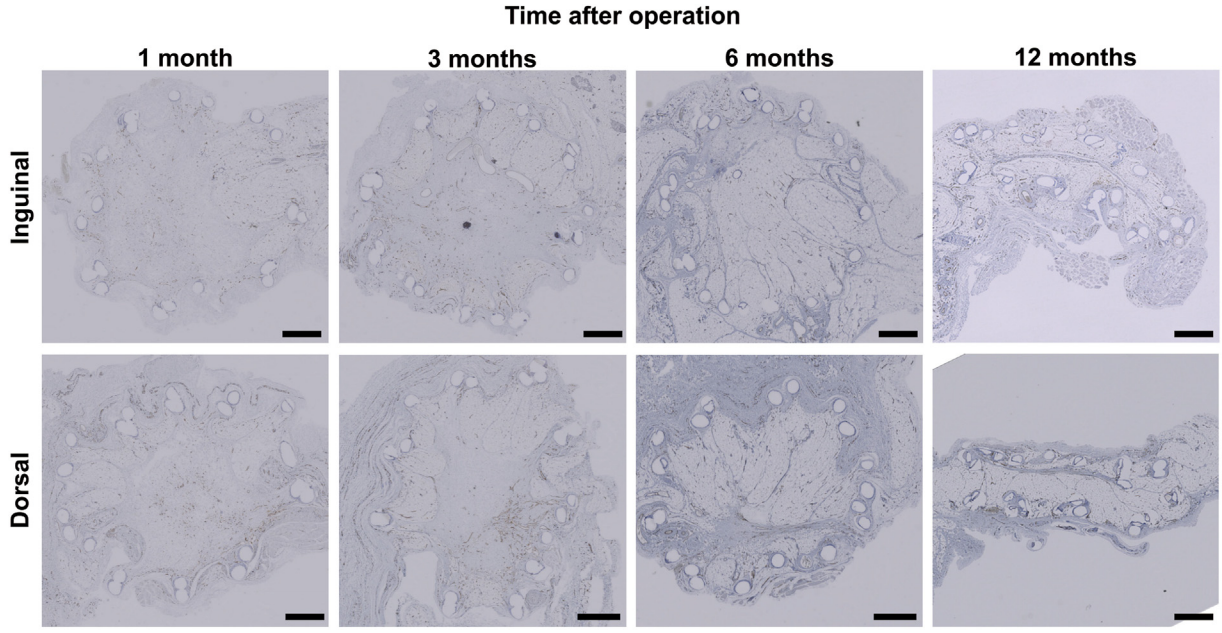

Fig. 6. Light micrographs of CD31-stained sections of the newly generated tissue. Many blood vessels were identified in adipose and non-adipose tissue areas inside the implant. Upper row: light micrographs in the inguinal model; lower row: light micrographs in the dorsal model. Scale bar = 1 cm.

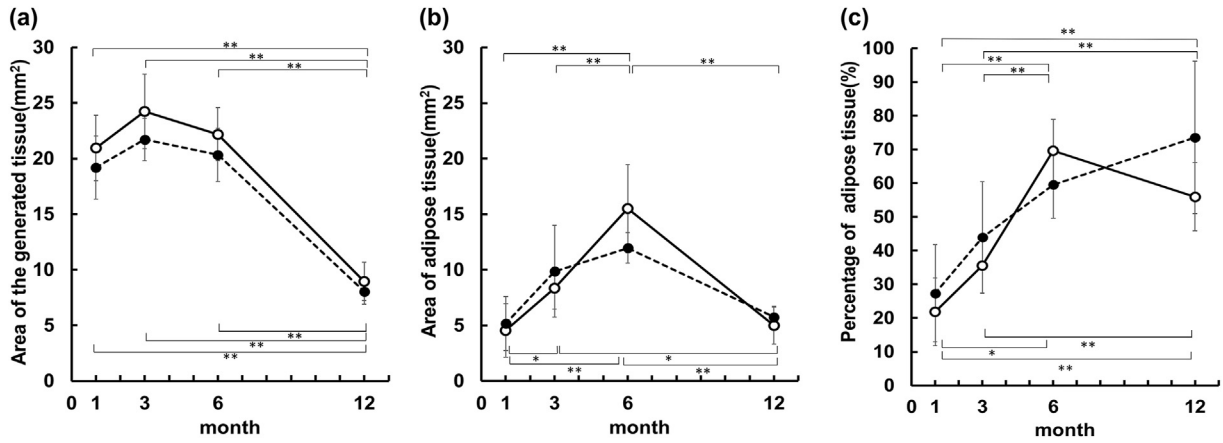

Fig. 7. Evaluation of the area of the newly generated and adipose tissues, as well as the percentage of adipose tissue inside the implants. (a) Area of the newly generated tissue inside the implant. In both inguinal and dorsal models, the area at 12 months after the operation was smaller than that at 1, 3, and 6 months. (b) Area of the newly generated adipose tissue inside the implant. In both the inguinal and dorsal models, the area peaked at 6 months for all observation points. (c) Percentage of adipose tissue in the newly generated tissue inside the implant. The percentage was maximum at 6 months in the inguinal model and increased till 12 months in the dorsal model. The upper *p-values* represent the inguinal model, and the lower *p-values* represent the dorsal model. Data are presented as the mean ± standard deviation. $*p < 0.05$, $**p < 0.01$. ○ = inguinal model;, ● = dorsal model.

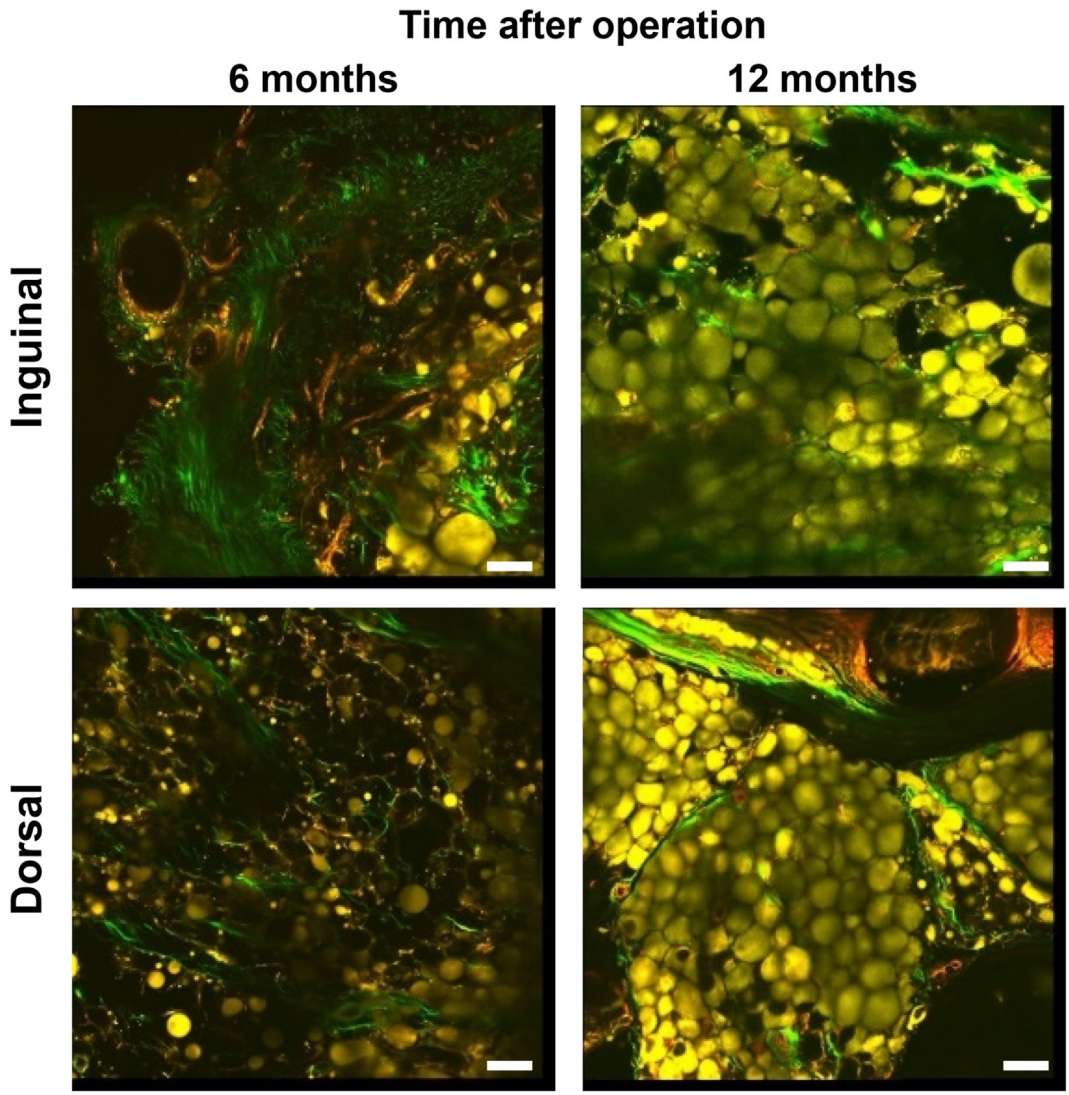

Fig. 8. Multiphoton images of newly generated tissue 6 and 12 months after the operation were collected at 860 nm. At 12 months, the size of the adipocytes was uniform and almost the same as the native adipocytes. Upper row: inguinal model (a) 6 months, (b) 12 months after operation. Lower row: dorsal model. (c) 6 months, (d) 12 months after operation. In each set: 30x image. The specimens were stained with NileRed (adipocytes; yellow), Isolectin GS-IB_4 from *Griffonia simplicifolia*, Alexa Fluor™ 488 Conjugate (blood vessels; red), and green shows SHG emission from collagen. Scale bars = 100 μm.

3.2. Histological assessment of the newly generated tissue and adipose tissue inside the implants

Micrographs of the H and E-stained sections of the newly generated tissue are shown in Fig. 4. In both the inguinal and dorsal models, the implant shape could be maintained for up to 6 months after the operation, but the implants were flattened 12 months after the operation. Micrographs of perilipin-stained sections of the newly generated tissue are shown in Fig. 5. In both the inguinal and dorsal models, the adipose tissue gradually increased from the edge of the implant after the operation. Micrographs of the CD31-stained sections of the newly generated tissue are shown in Fig. 6. Many blood vessels were identified in adipose and non-adipose tissue areas inside the implant.

3.3. Evaluation of the area of the newly generated tissue and adipose tissue inside the implant

The area of the newly generated tissue inside the implant is shown in Fig. 7a. In both inguinal and dorsal models, the area of newly generated tissue inside the implant at 12 months after the operation was smaller than that at 1, 3, and 6 months. The area of newly generated adipose tissue inside the implant is shown in Fig. 7b. In both the inguinal and dorsal models, the area of newly generated adipose tissue inside the implant peaked at 6 months for all observation points. The percentage of adipose tissue within the newly generated tissue inside the implant is shown in Fig. 7c. The percentage of adipose tissue was maximum at 6 months in the inguinal model and increased till 12 months in the dorsal model. There were no significant differences between the inguinal and dorsal models at any point in the areas and percentage.

3.4. Evaluation of the structure of the newly generated tissue using multiphoton excitation fluorescence microscopy

The cross-sections of newly generated tissue inside the implants are shown in Figs. 8 and 9. In Fig. 8, adipocytes were stained with Nile Red (yellow color), blood vessels were stained with isolectin (red color), and collagen was observed in the Second Harmonic Generation (green color). At 6 months after the operation, the size

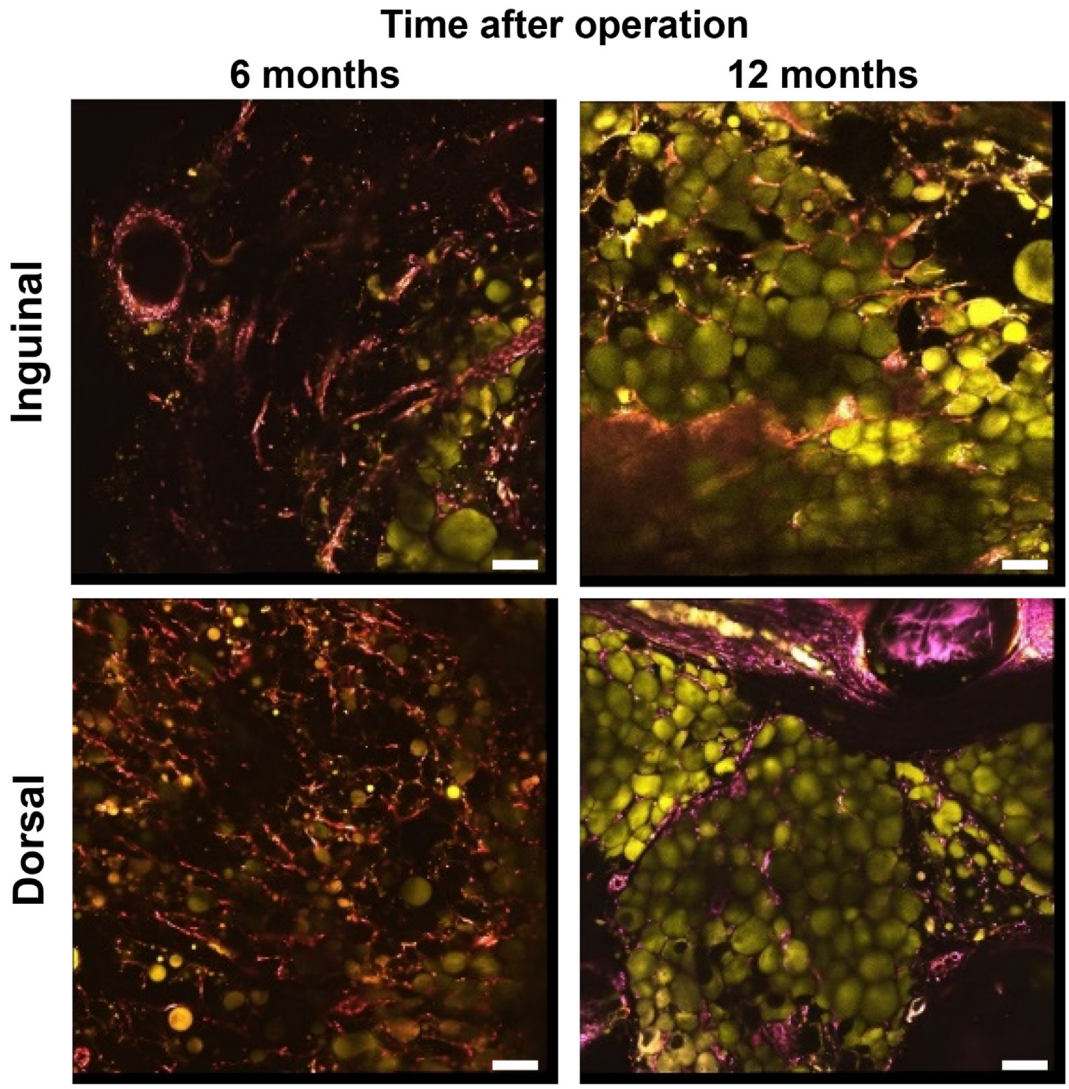

Fig. 9. Multiphoton images of native adipose tissue and newly generated tissue cross-sections at 6 and 12 months after the operation were collected at 760 nm. At 12 months, blood vessels surrounded the adipocytes, running in the tufts of adipose tissue with branches. Upper row: inguinal model (a) 6 months, (b) 12 months after the operation. Lower row: dorsal model (c) 6 months, (d) 12 months after the operation. In each set: 30x image. The specimens were stained with NileRed (adipocytes; yellow), Isolectin GS-IB_4 from *Griffonia simplicifolia*, Alexa Fluor™ 488 Conjugate (blood vessels; red), and Hoechst33342 (nuclei). Scale bars = 100 μm.

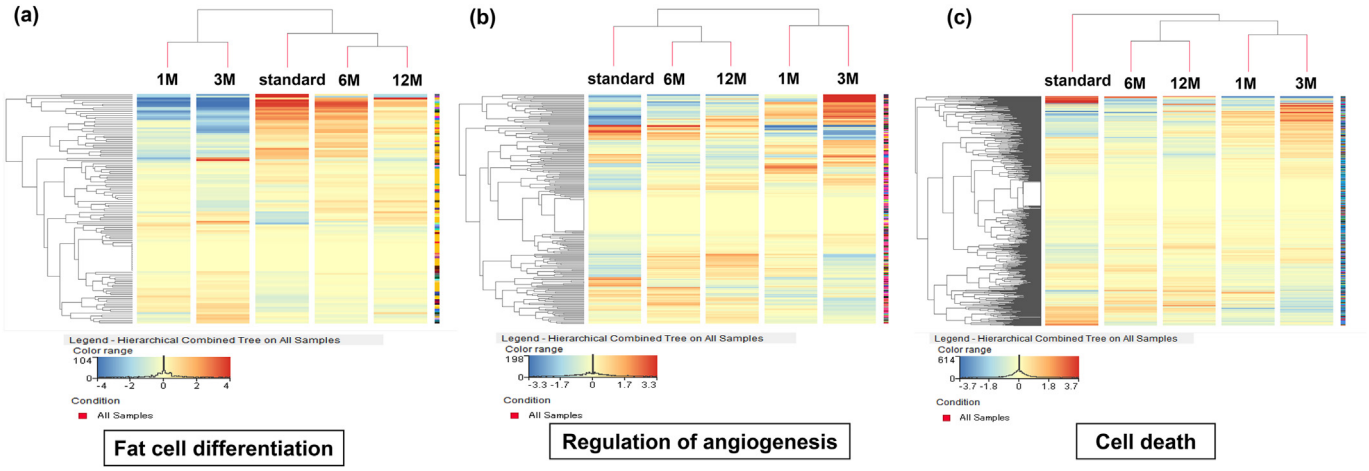

Fig. 10. RNA sequencing. (a) Adipogenic differentiation (GO term: Fat cell differentiation, gene number: 123). The expression of factors related to adipogenic differentiation was similar to that of normal adipose tissue from 6 months to 12 months after the operation, with a relatively low expression pattern at 12 months compared to that at 6 months after the operation. (b) Regulation of angiogenesis (GO term: Regulation of angiogenesis, gene number: 226). For genes involved in angiogenesis, high expression was observed from 1 to 3 months after the operation, but thereafter, as with normal adipose tissue, no significant expression was observed until 12 months after the operation. (c) Cell death (GO term: Cell death, gene number: 746). The gene expression was no increase related to apoptosis or necrosis at 6 and 12 months after the operation.

of the adipocytes was not uniform. Collagen quantity increased surrounding the PLLA and blood vessels. At 12 months, the size of the adipocytes was uniform and almost the same as the native adipocytes. Moreover, formed clusters like a mass resembling a bunch of grapes, surrounded by collagen in a net-like structure.

In Fig. 9, adipocytes were stained with Nile Red (yellow color), blood vessels were stained with isolectin (red color), and nuclei were stained with Hoechst33342 (blue color). Nuclei were located along the blood vessels, and the red and blue colors overlapped, causing them to appear purple color. At 12 months, blood vessels surrounded the adipocytes, running in the tufts of adipose tissue with branches.

3.5. RNA-seq

Adipogenesis-related gene expression was similar to that of normal adipose tissue from 6 months to 12 months, with a relatively low expression pattern at 12 months compared to that at 6 months (Fig. 10a). Angiogenesis-related gene expression was observed from 1 to 3 months after the operation, but thereafter, as with normal adipose tissue, no significant expression was observed until 12 months after the operation (Fig. 10b). This result was consistent with the histological findings that the implants flattened at 12 months. No significant expression in cell death-related gene expression was observed at 6 and 12 months (Fig. 10c).

4. Discussion

In this study, we evaluated adipogenesis over time in our implants both histologically and in terms of gene expression related to adipogenesis, angiogenesis, and cell death. In the peripheral area, newly generated adipose tissue began to be observed at 1 month, increased gradually, and was uniformly distributed inside implants at 6 months (Fig. 5). However, the amount of adipose tissue decreased from 6 months until 12 months. As for the angiogenesis, the expression of genes related to angiogenesis was observed until 3 months. These suggest that angiogenesis inside implants developed within the first 3 months, and adipose tissue differentiated at 6 months. The amount of adipose tissue began to decrease after 6 months; however, mature adipose tissue remained after 12 months, and cell death-related gene expression was not elevated at 12 months. Multiphoton imaging showed that at 12 months, both adipose tissue and blood vessels matured the same as the native adipose tissue (Figs. 8 and 9), suggesting consistency in the results obtained from RNA-seq and multiphoton imaging for adipogenesis and angiogenesis analyses.

As for the decrease in the amount of newly generated adipose tissue, the area of the newly generated tissue decreased significantly from 6 to 12 months. On the other hand, the percentage of adipose tissue in implants did not decrease from 6 to 12 months, likely because implants collapsed after 6 months and no longer maintained their internal structure. Therefore, we must reinforce the structure of implants to sustain the newly generated adipose tissue.

We confirmed that our bioabsorbable implants could induce adipogenesis into themselves both in the inguinal and the dorsal regions without significant difference just after implantation until one year. We could not anticipate this result, because subcutaneous tissue in the dorsal region was membranous, with only a little adipose tissue. This result indicated that the adipose tissue could be formed inside the implants even if a small amount of adipocytes was present in the surrounding area. Therefore, this implant might be used in the sites after total mastectomy or under the pectoralis major muscle.

The regeneration of adipose tissue using bioabsorbable materials is reported using polycaprolactone-based scaffolds in a porcine model [27] or poly-4-hydroxybutyrate mesh scaffolds in a clinical trial [28] by combining with autologous fat transfer. Our implants, without the addition of growth factors or cells, pose no risk of recurrence and metastasis. Furthermore, for the absorbance of PLLA threads within a few years, our PLLA implants are less likely to induce BIA-ALCL and can be a novel and safe material for breast reconstruction after mastectomy. However, in the future, we need to confirm the safety of our implants in detail.

The limitation of this study is that in our previous work, the shape of the implant was maintained for up to 12 months after the operation. However, the shape of the implant was only maintained for 6 months in this study. This might have occurred because of concurrent inguinal and dorsal implantation operations. Thus, the decrease in regenerated adipose tissue at 12 months may be due to the failure of the implant to maintain its shape rather than cell death, and the newly generated tissue inside the implant might

deviate from the implant. We plan to investigate the difference in circumstances such as tissue pressure, between rat models and in clinical application after mastectomy. The ultimate aim is to develop a new implant that can maintain its structure for a longer period while fostering adipogenesis. In the future, we will investigate adipogenesis of our implants using animals with longer lifespans for a long-term observation period.

5. Conclusions

Our bioabsorbable implant is a novel bioabsorbable that is replaced by adipose tissue after the operation, regardless of the presence of a small amount of adipocytes in the surrounding area. We showed that the newly generated adipose tissue had the same morphology as native adipose tissues. Our implants can be a novel method for breast reconstruction and to improve patients' quality of life.

Author contributions

S. L. and N. M. designed the study. Y. K. prepared the materials, while S. L., K. Y., Y. K., M. C. M., and M. S. performed the experiments. S. L., S. O., Y. S., K. Y., M. C. M, S. S., M. S., T. Y., and N. M. analyzed the data. S. L., S. O., and N. M. wrote and revised the manuscript. N. M. was the grant recipient.

Ethics statement

We performed our experiments at the Institute of Laboratory Animals, Graduate School of Medicine, Kyoto University, Japan, where the experimental animals were housed. The protocol was designed in accordance with the ARRIVE guidelines and was approved by the university's Animal Research Committee (permit number: Med Kyoto 19,124. We attempted to minimize the number of rats used and reduce animal suffering following the protocol established by the Animal Research Committee of Kyoto University.

Data availability statement

The datasets generated during and/or analyzed during the current study are available from the corresponding author upon reasonable request.

Declaration of competing interest

The authors report no proprietary or commercial interest in any product mentioned or concept discussed in this article.

Acknowledgments

This work was supported by the AMED (Grant JP21hm0 102068h0003). Medical Science for support in conducting the animal experiments, and Editage (www.editage.com) for English language editing.

References

[1] Silverman BG, Brown SL, Bright RA, Kaczmarek RG, Arrowsmith-Lowe JB, Kessler DA. Reported complications of silicone gel breast implants: an epidemiologic review. Ann Intern Med 1996;124:744–56.
[2] Brown SL, Silverman BG, Berg WA. Rupture of silicone-gel breast implants: causes, sequelae, and diagnosis. Lancet 1997;350:1531–7.
[3] Kim B, Predmore ZS, Mattke S, van Busum K, Gidengil CA. Breast implant-associated anaplastic large cell lymphoma: updated results from a structured expert consultation process. Plast Reconstr Surg Glob Open 2015;3:e296.
[4] Alotaibi S, Hamadani M, Al-Mansour M, Aljurf M. Breast implant-associated anaplastic large cell lymphoma. Clin Lymphoma, Myeloma Leukemia 2021;21:e272–6.
[5] Ellenbogen R. Free autogenous pearl fat grafts in the face–a preliminary report of a rediscovered technique. Ann Plast Surg 1986;16:179–94.
[6] Gir P, Oni G, Brown SA, Mojallal A, Rohrich RJ. Human adipose stem cells: current clinical applications. Plast Reconstr Surg 2012;129:1277–90.
[7] von Heimburg D, Zachariah S, Heschel I, Kuhling H, Schoof H, Hafemann B, et al. Human preadipocytes seeded on freeze-dried collagen scaffolds investigated in vitro and in vivo. Biomaterials 2001;22:429–38.
[8] Glowacki J, Mizuno S. Collagen scaffolds for tissue engineering. Biopolymers 2008;89:338–44.
[9] Kimura Y, Ozeki M, Inamoto T, Tabata Y. Time course of de novo adipogenesis in matrigel by gelatin microspheres incorporating basic fibroblast growth factor. Tissue Eng 2002;8:603–13.
[10] Kimura Y, Ozeki M, Inamoto T, Tabata Y. Adipose tissue engineering based on human preadipocytes combined with gelatin microspheres containing basic fibroblast growth factor. Biomaterials 2003;24:2513–21.
[11] Hiraoka Y, Yamashiro H, Yasuda K, Kimura Y, Inamoto T, Tabata Y. In situ regeneration of adipose tissue in rat fat pad by combining a collagen scaffold with gelatin microspheres containing basic fibroblast growth factor. Tissue Eng 2006;12:1475–87.
[12] Tsuji W, Inamoto T, Yamashiro H, Ueno T, Kato H, Kimura Y, et al. Adipogenesis induced by human adipose tissue-derived stem cells. Tissue Eng 2009;15:83–93.
[13] Choi YS, Cha SM, Lee YY, Kwon SW, Park CJ, Kim M. Adipogenic differentiation of adipose tissue derived adult stem cells in nude mouse. Biochem Biophys Res Commun 2006;345:631–7.
[14] Muehlberg FL, Song YH, Krohn A, Pinilla SP, Droll LH, Leng X, et al. Tissue-resident stem cells promote breast cancer growth and metastasis. Carcinogenesis 2009;30:589–97.
[15] Chandler EM, Seo BR, Califano JP, Andresen Eguiluz RC, Lee JS, Yoon CJ, et al. Implanted adipose progenitor cells as physicochemical regulators of breast cancer. Proc Natl Acad Sci U S A 2012;109:9786–91.
[16] Alperovich M, Lee ZH, Friedlander PL, Rowan BG, Gimble JM, Chiu ES. Adipose stem cell therapy in cancer reconstruction: a critical review. Ann Plast Surg 2014;73(Suppl 1):S104–7.
[17] Rowan BG, Gimble JM, Sheng M, Anbalagan M, Jones RK, Frazier TP, et al. Human adipose tissue-derived stromal/stem cells promote migration and early metastasis of triple negative breast cancer xenografts. PLoS One 2014;9:e89595.
[18] Kolle SF, Fischer-Nielsen A, Mathiasen AB, Elberg JJ, Oliveri RS, Glovinski PV, et al. Enrichment of autologous fat grafts with ex-vivo expanded adipose tissue-derived stem cells for graft survival: a randomised placebo-controlled trial. Lancet 2013;382:1113–20.
[19] Kakudo N, Morimoto N, Ogawa T, Hihara M, Lai F, Kusumoto K. Adipose-derived stem cell (ASC)-enriched fat grafting: experiments using White rabbits and an automated cell processing apparatus. Med Mol Morphol 2017;50:170–7.
[20] Storti G, Scioli MG, Kim BS, Terriaca S, Fiorelli E, Orlandi A, et al. Mesenchymal stem cells in adipose tissue and extracellular vesicles in ovarian cancer patients: a bridge toward metastatic diffusion or a new therapeutic opportunity? Cells 2021:10.
[21] Greenberger S, Bischoff J. Pathogenesis of infantile haemangioma. Br J Dermatol 2013;169:12–9.
[22] Smith CJF, Friedlander SF, Guma M, Kavanaugh A, Chambers CD. Infantile hemangiomas: an updated review on risk factors, pathogenesis, and treatment. Birth Defects Res 2017;109:809–15.
[23] Tsuji W, Inamoto T, Ito R, Morimoto N, Tabata Y, Toi M. Simple and long-standing adipose tissue engineering in rabbits. J Artif Organs 2013;16:110–4.
[24] Ogino S, Morimoto N, Sakamoto M, Jinno C, Yoshikawa K, Enoshiri T, et al. Development of a novel bioabsorbable implant that is substituted by adipose tissue in vivo. J Tissue Eng Regen Med 2018;12:633–41.
[25] Mian R, Morrison WA, Hurley JV, Penington AJ, Romeo R, Tanaka Y, et al. Formation of new tissue from an arteriovenous loop in the absence of added extracellular matrix. Tissue Eng 2000;6:595–603.
[26] Bourne R. ImageJ. Fundamentals of digital imaging in medicine. London: Springer London; 2010. p. 185–8.
[27] Chhaya MP, Balmayor ER, Hutmacher DW, Schantz JT. Transformation of breast reconstruction via additive biomanufacturing. Sci Rep 2016;6:28030.
[28] Rehnke RD, Schusterman 2nd MA, Clarke JM, Price BC, Waheed U, Debski RE, et al. Breast reconstruction using a three-dimensional absorbable mesh scaffold and autologous fat grafting: a composite strategy based on tissue-engineering principles. Plast Reconstr Surg 2020;146:409e. 13e.